



# Ultrathin polytyramine films by electropolymerisation on highly doped p-type silicon electrodes

Dusan Losic<sup>a</sup>, Martin Cole<sup>a</sup>, Helmut Thissen<sup>b</sup>, Nicolas H. Voelcker<sup>a,\*</sup>

<sup>a</sup> School of Chemistry, Physics and Earth Sciences, Flinders University, GPO Box 2100, Bedford Park, SA 5042, Australia

<sup>b</sup> CSIRO Molecular Science, Clayton VIC 3168, Australia

Received 21 December 2004; accepted for publication 4 April 2005

Available online 18 April 2005

## Abstract

In recent years, silicon-based materials have been used extensively in device fabrication for sensors, microfluidic and biomaterial applications. In order to enhance the performance of the material, a number of surface functionalisations are employed. However, until now, silicon has not been used as an electrode material for electrodeposition of functional polymers. Here, highly doped p-type silicon was used as an electrode facilitating the electropolymerisation of ultrathin polytyramine (PT) films by cyclic voltammetry. The influence of resistivity, pre-treatment of the silicon surface and electrochemical conditions on the electropolymerisation process was studied. The results show that ultrathin PT films with a controlled thickness from 2 to 15 nm exhibit good electrochemical stability in buffer solution (pH 6.8) over a large potential window (−1.5 V to 1.5 V) and passivating properties towards a redox probe. In terms of the film morphology, a pinhole-free smooth surface with a roughness below 0.5 nm and with dominantly globular features of 40–60 nm diameter was observed by AFM. XPS characterisation showed that PT films display amine functional groups at the coating surface. UV induced silicon oxidation was used to prepare patterned PT films.

© 2005 Elsevier B.V. All rights reserved.

**Keywords:** Silicon; Electrochemical methods; Electropolymerisation; Growth; Cyclic voltammetry; Surface chemical reaction; Polytyramine; Atomic force microscopy; Surface structure; X-ray photoelectron spectroscopy; Insulating films

## 1. Introduction

Silicon is technologically one of the most important industrial materials and significant research efforts have been devoted over the past two decades to further advance its electronic, optical, chemical and physical properties. Interfacing with organic

\* Corresponding author. Tel.: +61 8 82015338; fax: +61 8 82012905.

E-mail address: [nico.voelcker@flinders.edu.au](mailto:nico.voelcker@flinders.edu.au) (N.H. Voelcker).

and biological materials in particular has become the subject of vigorous investigations to enable target applications in molecular electronics and biondiagnostics [1,2]. Self-assembled monolayers (SAMs) from silanes and Si–C bond forming reactions have been the most accepted approach for surface modification of silicon [3,4]. However, ultrathin films of organic polymers are considered an attractive alternative approach for modification of silicon surfaces [5]. Organic films on silicon can serve as an effective etching barrier, yield chemical and mechanical protection, alter the chemical and electrical properties of the underlying surface, reveal new properties such as conductivity, photo- and electroluminescence, and provide new pathways to functionalisation of silicon for molecular recognition and sensing devices [6,7].

In general, polymer films on silicon surfaces are prepared using deposition techniques such as physical dispersion (spin coating), chemical vapour deposition (CVD), plasma deposition, as well as chemical or electrochemical reactions [8–10]. Notably, the latter do not require high-vacuum conditions, can be performed in an aqueous environment and at ambient temperatures. Electrochemical methods also provide a high degree of control over polymer growth and film thickness with good reproducibility [11]. The majority of studies on electropolymerisation reported in the literature have for obvious reasons focused on highly conductive electrodes such as gold, platinum, and carbon [11,12]. Fabrication of a variety of both conductive (polyaniline, polypyrrole, polythiophene) and nonconductive (polyphenol, polytyramine) polymer films and their copolymers was demonstrated over the past two decades [12–14]. Silicon, however, poses a challenge as an electrode material because of its resistivity and the insulating properties of its oxide layer [7,15,16]. In the last few years, electrochemistry on silicon, including porous silicon, has received greater attention with a number of groups reporting electrochemical methods for grafting of organic layers on silicon [4,17–21]. We recognised that it is important to choose appropriate electrochemical reactions to find the accessible redox potential, in order to exploit the electrochemical reactivity of silicon [15,17,20].

Our research group is interested in functional silicon devices for drug delivery and biosensing and we are investigating electropolymerisation as a means to deliver functional organic films on silicon and porous silicon [22,23]. We have chosen low resistivity and highly boron doped silicon ( $p^{++}$ , resistivity  $<0.001 \Omega \text{ cm}$ ) wafers as our electrode material, and have studied their applicability for electropolymerisation and fabrication of ultrathin polymer films. Tyramine was chosen as a monomer because of its pendant amine group which is known to be electroinactive. The amine functional group can be used for covalent attachment of organic molecules and biomolecules of interest [24–26]. The electropolymerisation of tyramine on gold has been described in previous work and in addition has been studied on other substrates such as platinum, and glassy carbon [26–29]. This study is the first demonstration of polytyramine (PT) electropolymerisation on silicon surfaces. Cyclic voltammetry, ellipsometry, X-ray photoelectron spectroscopy (XPS) and atomic force microscopy (AFM) characterisation were employed to address several important issues of the electropolymerisation process such as the pre-treatment of the silicon electrode, the silicon resistivity, the influence of electrochemical parameters as well as the PT film stability and morphology.

## 2. Materials and methods

### 2.1. Materials

Two types of silicon wafers, p-type ( $p^{++}$ -Si), boron doped, orientation  $\langle 100 \rangle$ , and 76.2 mm diameter with low resistivity  $0.0005\text{--}0.001 \Omega \text{ cm}$ , and medium resistivity p-type (p-Si)  $3\text{--}5 \Omega \text{ cm}$ , were obtained from Virginia Semiconductors (USA) and Silicon Quest (USA), respectively. Gold foil (99.95) was supplied from Peter W. Beck Pty. Ltd Adelaide, Australia. Tyramine (4-hydroxyphenylethylamine) and 40%  $\text{NH}_4\text{F}$  solution (semiconductor grade) was purchased from Aldrich (Australia). Potassium ferricyanide, potassium chloride, potassium dihydrogen orthophosphate and dipotassium hydrogen orthophosphate

were supplied by Ajax Chem Pty. Ltd. (Sydney, Australia). Other chemicals were of the highest quality commercially available and were used without further purification. All aqueous solutions were prepared with ultra-pure Milli Q grade water (18.2 M $\Omega$ ) and filtered through a 100 nm porous alumina filter (Whatmann).

## 2.2. Electropolymerisation of tyramine on silicon

The silicon wafers were cut into pieces (15 mm  $\times$  15 mm) and ultrasonically cleaned for a minimum of 10 min in analytical grade chloroform, acetone, ethanol and ultra-pure water followed by drying with a stream of filtered nitrogen. To investigate the influence of the chemical nature of the silicon surface on the polymerisation process, we prepared both oxidised and hydrogen-terminated silicon by standard procedures [32]. Briefly, to produce oxidised silicon, ultrasonically cleaned silicon was treated in a mixture of concentrated sulphuric acid (98%) and 30% aqueous H<sub>2</sub>O<sub>2</sub> solution 7:3 (v:v) (Piranha solution) for 5–10 min, followed by extensive washing with Milli Q water and drying with a stream of nitrogen. This treatment provides a hydrophilic, highly oxidised silicon surface capped with silanol groups. To produce a hydrophobic, hydride terminated surface, the Piranha treated silicon was etched with 2% HF for 1 min to remove the oxide layer, and then etched in deoxygenated 40% NH<sub>4</sub>F solution for 15 min, followed by careful drying under a nitrogen stream [32].

The electrochemical polymerisation of tyramine on silicon substrates was performed using a Power Lab, Model 400 S (AD Instruments, Sydney Australia) computer-controlled electrochemical system. Custom-made Teflon electrochemical cells were used with cavity diameters of 4 mm, 6 mm and 10 mm as described in previous work [33]. An Ag/AgCl/saturated KCl served as the reference electrode and a platinum mesh (diameter 12 mm) as the auxiliary electrode. The monomer solution consisted of 0.1 M tyramine in phosphate buffer/methanol solution (3:1) 0.05 M, pH 6.8, at room temperature. The solution was purged with nitrogen for at least 20 min prior to potential cycling and blanketed with argon throughout the experiment. Current–voltage cyclic voltammetric (CV)

graphs were recorded versus the reference electrode using a personal computer and Echem software (AD instruments) The applied potential during polymerisation was cycled between 0 V and +1.5 V versus Ag/AgCl; the scan rate was varied from 10 mV s<sup>-1</sup> to 500 mV s<sup>-1</sup> and 1, 5, 10 and 20 sweep cycles were applied. CV graphs were taken for each cycle and presented as *I/V* curves. Current density was calculated from the measured current and the effective electrode area. After polymerisation, polytyramine/silicon (PT/Si) samples were thoroughly rinsed with methanol-phosphate buffer to remove unreacted monomer from the surface, followed by rinsing in Milli Q water and drying using a stream of nitrogen for 1 min. A comparative polymerisation on a gold electrode and high resistivity silicon (3–5  $\Omega$  cm) was performed using the same conditions as described above.

The fabrication of patterned polytyramine films was performed on a NH<sub>4</sub>F-treated, Si–H terminated silicon surface. Prior to polymerisation, silicon was irradiated with UV light through a mask (metal grids with 50  $\mu$ m square holes) over 24 h. The light source used was a mercury arc lamp with a power of 100 W (Oriel, USA). Electropolymerisation was performed (100 mV s<sup>-1</sup>, 20 deposition cycles) immediately after irradiation followed by thorough rinsing as described above.

## 2.3. Characterisation of PT films on silicon

Ellipsometry measurements of the thickness of PT films on silicon were performed using an ellipsometer SE 40, Sentech Instrument (Germany) equipped with a 632.8 nm Helium/Neon laser at a 70° incident angle. The reflected light is analysed at a fixed analyser position using a multi-channel analyser. The thickness is measured from ellipsometry data assuming a double-layer model (silicon substrate + silicon oxide layer + PT layer). The following refractive indexes were used: 3.88816 for native silicon, 1.462 for silicon oxide and 1.466 for PT layer. The results presented are averaged from a minimum of five measurements. The surface coverage  $\Gamma$  (mg m<sup>-2</sup>) was calculated using the equation  $\Gamma = h \cdot \delta$ , where  $h$  is the thickness of the layer, and  $\delta = 1.1$  g cm<sup>3</sup> is the mass density of PT [34].

X-ray photoelectron spectroscopy (XPS) analysis of surface modified samples was performed on an AXIS HSi spectrometer (Kratos Analytical Ltd.), equipped with a monochromatized  $\text{AlK}_{\alpha}$  source. The pressure during analysis was typically  $5 \times 10^{-8}$  mbar. The elemental composition of samples was obtained from survey spectra, collected at a pass energy of 320 eV. High resolution spectra were collected at a pass energy of 40 eV. In order to quantify contributions to the C1s and N1s peaks from chemically different species, curve fitting of the corresponding high resolution spectra was performed using Vision 1.5, the data processing software supplied with our instrument (Kratos Analytical Ltd.). The curve fit protocol employed Gaussian/Lorentzian product functions (20–30% Lorentzian, 70–80% Gaussian), each defined by position, width and height, and used a Simplex algorithm for the actual minimisation. In the case of C1s spectra, all peak components were constrained to have the same, but variable, width. No other constraints were applied. Binding energies were referenced to the aliphatic carbon peak at 285.0 eV.

The electrochemical stability and the passivating properties of PT films were investigated by cyclic voltammetry using an approach developed for the assessment of the integrity of SAMs on gold [35,36]. Firstly, wide potential range CVs (from  $-1.5$  V to  $+1.5$  V) and subsequent potential cycling (1–20 cycles) tested the stability of PT films on silicon in phosphate buffer 50 mM, pH 6.8. Secondly, the redox probe ferricyanide (0.05 mM in 0.1 M KCl) was used to probe the integrity of PT film in a CV experiment from 0 to  $-1.3$  V, a scan rate of  $100 \text{ mV s}^{-1}$  and three successive cycles. Comparison of the reduction peak current on bare Si and PT films was used for assessment of electrochemical passivation.

Atomic force microscopy (AFM) was performed on a Multi Mode, Nanoscope IV Digital Instruments microscope (Veeco Corp. Santa Barbara, USA) in both tapping and contact mode in air. Ultra-Sharp (NT-MDT, Moscow, Russia) silicon tips with 150–350 kHz resonance frequencies were used for tapping mode and silicon nitride tips (DI Instrument) with a nominal spring constant of  $0.58\text{--}5.5 \text{ N m}^{-1}$  were used for contact mode. Im-

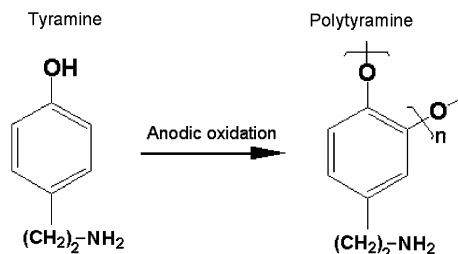
aged areas for each sample were  $5 \mu\text{m} \times 5 \mu\text{m}$ ,  $2 \mu\text{m} \times 2 \mu\text{m}$  and  $1 \mu\text{m} \times 1 \mu\text{m}$ . Roughness ( $R_a$ ) measurements, which represent the mean value of the roughness curve relative to the centre line, were taken from  $2 \mu\text{m} \times 2 \mu\text{m}$  images. The film thickness of PT films was measured by the “scratching method” using high loading force contact mode ( $>50 \text{ nN m}^{-1}$ ). Image processing was performed using DI off-line software (Veeco Corp. Santa Barbara, USA) and SPIP software (Image Metrology, Denmark).

### 3. Results and discussion

#### 3.1. Electrochemical polymerisation of tyramine on $p^{++}$ -silicon

The electropolymerisation of tyramine on highly doped p-silicon was performed using cyclic voltammetry. The oxidation of tyramine occurs through the *ortho* position, similar to electrochemical polymerisation of other phenols [14]. The basic reaction is shown in Scheme 1. The process involves several steps including anodic oxidation of tyramine monomers, formation of radical cations, oligomerisation, nucleation of oligomers on the surface and polymer growth on the surface.

A typical cyclic voltammogram (CV) for the oxidative polymerisation of tyramine on low resistivity ( $<0.001 \Omega \text{ cm}$ ) silicon in phosphate buffer/methanol solution (pH 6.8) is presented in Fig. 1A. The graph (1 cycle) shows that oxidation of tyramine is completely irreversible and only a broad anodic peak is observed in the potential range from  $+0.5$  V to  $+1.2$  V with a maximum at



Scheme 1. Schematic of the electrooxidation/polymerisation of tyramine.

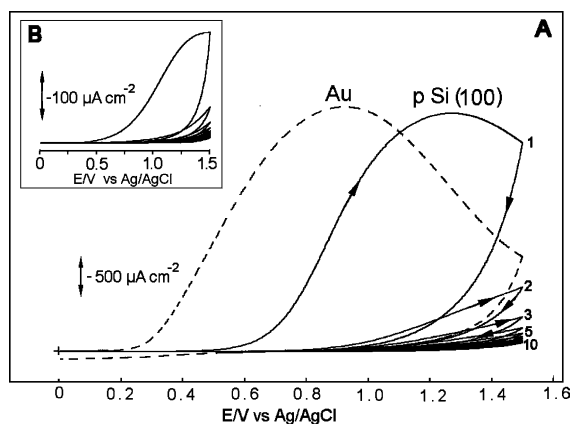


Fig. 1. (A) Cyclic voltammograms (full line) for electrooxidation of tyramine on a highly doped silicon electrode ( $p^{++}\text{-Si}$  (100), ultrasonically cleaned) at a scan rate of  $100 \text{ mV s}^{-1}$  versus Ag/AgCl in 0.05 M tyramine in 0.05 M phosphate buffer/methanol solution (3:1, pH 6.8). Comparative cyclic voltammogram (dashed line) on a gold electrode using same conditions (only first scan is shown). (B) Cyclic voltammograms on a silicon electrode ( $p^{++}\text{-Si}$  (100), ultrasonically cleaned) in supporting electrolyte (phosphate/methanol) without of tyramine obtained at a scan rate of  $100 \text{ mV s}^{-1}$  versus Ag/AgCl.

1.3 V. In the second and subsequent scans, the peak current dropped significantly with each cycle until complete suppression of the electrodeposition current was observed after 10 scans. This observation indicates that an insulating and passivating polymeric film is formed on the silicon surface. For comparison, a CV (first oxidation scan) of the electropolymerisation of tyramine on a gold electrode is shown in Fig. 1A (dashed line). Similar CVs and the general trend of decreasing anodic current by subsequent cycling are also observed on platinum and glassy carbon electrodes [24–29]. We observed that electrooxidation of tyramine on the gold electrode starts at lower potentials (onset at +0.1 to +0.2 V) and reached peak current at +0.7 to +0.9 V. Normalised to the same electrochemically active area, ca. 20% more polytyramine is deposited on gold than on our silicon wafers. The discrepancy in peak potential and intensity of oxidation process between highly doped silicon and gold could be related to the semiconductive properties of silicon and the presence of a thin, poorly conductive oxide layer on the surface (2 nm). It is well known that the presence of an

oxide layer can induce dramatic changes in the electrochemical behaviour of an electrode [15,36]. Due to charge-transfer limitations at the silicon oxide layer/solution interface, the oxidation of tyramine is likely to require a higher potential. However, we noted that the electrooxidation process is not prevented by the likely presence of an oxide layer on ultrasonically cleaned silicon. This key observation led us to pursue highly doped p-type silicon as an electrode material for electropolymerisation.

The electroactivity of the silicon electrode in aqueous electrolyte was expected to impact on the electropolymerisation process. Anodisation of silicon in aqueous medium will unavoidably result in the formation of a layer of silicon dioxide or, in the presence of certain electrolytes (fluorides for example), lead to the dissolution of silicon and the formation of pores [4,37]. To investigate the electrochemical reactivity of highly doped silicon electrodes under our electropolymerisation conditions, the CVs in supporting electrolyte solution omitting tyramine were recorded. Fig. 1B shows CVs on silicon obtained in phosphate buffer/methanol solution (pH 6.8) at  $100 \text{ mV s}^{-1}$  and 10 sweep cycles. These CVs show an increase in the current at potentials above 0.6 V and reach a maximum between 1.2 and 1.3 V, which is attributed to the oxidation process of silicon. The drop in current with the number of voltammetric scans is consistent with the formation of a poorly conductive silicon oxide layer. When degassing of buffer solution is omitted, the intensive surface oxidation results in an 15–20% increased oxidation peak current (data not shown). Comparative XPS analysis of the silicon surface before and after cycling, showed an increase of the O 1s peak, which is consistent with  $\text{SiO}_2$  formation (data not shown). These results suggest that some oxidation of the silicon electrode cannot be avoided during the electropolymerisation of tyramine. However, the observed current density of silicon oxidation in buffer solution ( $285 \pm 55 \mu\text{A cm}^{-2}$ ) is about one order of magnitude lower than the current density for tyramine oxidation on silicon ( $2432 \pm 300 \mu\text{A cm}^{-2}$ ). We can therefore conclude that electrooxidation of tyramine was the dominant process in the CV shown in Fig. 1A.

### 3.2. Characterisation of the PT films

XPS measurements were conducted to confirm the presence of PT films on silicon. The survey spectrum in Fig. 2A shows the presence of four elements silicon, carbon, oxygen and nitrogen. The observed chemical composition of the PT films on silicon was in reasonable agreement with expected theoretical values based on the chemical structure of polytyramine (C 80%, N 10%, O 10%). The excess of oxygen relative to nitrogen (experimental O/N ratio of 2.5) is due to additional Si–O and C–O components. Table 2 shows the quantification of XPS spectra recorded at different photoemission angles ( $0^\circ$  and  $70^\circ$ ). Depth profiling by angle-resolved (or angle-dependent) XPS (ARXPS) is based on the exponential attenuation of the photoelectron signal while passing through solid material according to the Beer–Lambert law. The sampling depth can therefore be varied by changing the angle at which the ejected photoelectrons are detected according to  $d = 3\lambda \cos \Theta$ , where  $d$  is the sampling depth (defined as the thickness of the surface layer from which approximately 95% of the total photoelectron intensity originates,

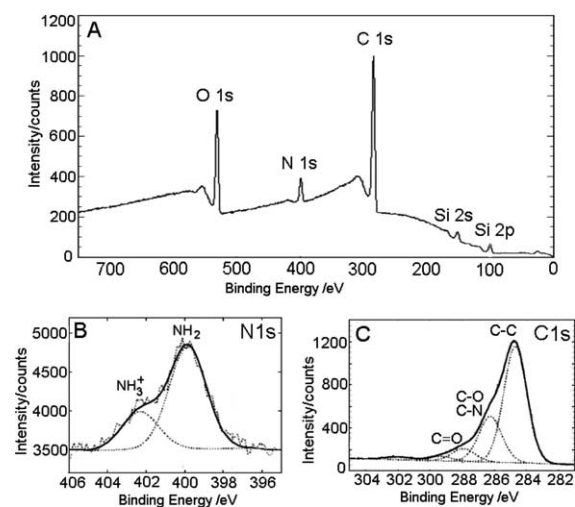


Fig. 2. XPS spectra of PT film electrochemically deposited on silicon (ultrasonically cleaned  $p^{++}$ -Si (100)) from 0.05 M tyramine in phosphate buffer/methanol (3:1, pH 6.8) obtained using a potential scan width: 0–1.5 V, scan rate:  $100 \text{ mV s}^{-1}$  versus Ag/AgCl and 10 deposition cycles. (A) survey spectrum, (B) N 1s XPS spectrum and (C) C 1s spectrum.

i.e. approximately three times the attenuation length);  $\lambda$  is the electron attenuation length and  $\Theta$  the emission angle (with respect to the surface normal). Assuming an attenuation length of 4.0 nm for Si 2p photoelectrons in organic materials [30], the sampling depth is of the order of 12 nm ( $0^\circ$  emission angle) and 4 nm ( $70^\circ$  emission angle) respectively. At a photoemission angle of  $70^\circ$ , we observed a reduction of the silicon content from 5.7% to 1.2% and a slight decrease of the O/N ratio to a value of 2.2.

The high-resolution C 1s spectrum was fitted with four peaks which were assigned to the chemical environments C–C/C–H, C–O/C–N, C=O and O–C=O. In addition, a peak at higher binding energy resulting from the aromatic structure of tyramine was observed (Fig. 2C). The presence of several oxidised carbon species explains, at least in part, the observed discrepancy of the theoretical and experimental N/O atomic ratio. The origin of C=O and O–C=O species may be assigned to by-products of the anodic oxidation of tyramine described in Scheme 1. The N 1s spectrum in Fig. 2B shows two peaks at 399.8 eV and 401.7 eV, respectively, corresponding to neutral amine ( $-\text{NH}_2$ ) and protonated amine ( $-\text{NH}_3^+$ ). The observation of partially protonated amines is expected under the conditions used in our study. However, oxidised nitrogen species, which appear at much higher binding energies, were not observed. The absence of oxidised nitrogen species in the high resolution N 1s spectra confirms that the amino group of tyramine is not involved in the electropolymerisation reaction [24,25]. This is in contrast to other surface functionalisation methods such as plasma polymerisation of amino-functional monomers, where the formation of various oxidised nitrogen species cannot be avoided [22,23].

A typical AFM image of the PT film on ultrasonically cleaned silicon after 10 CV cycles is shown in Fig. 3A. Whilst the topography was significantly different from silicon, the surface still appeared smooth with a mean roughness of 0.35 nm as compared to 0.20 nm for silicon. Small globular structures with lateral dimensions of 30–40 nm and an average height of about 1 nm were the dominant features on the surface (inset Fig. 3A). Using

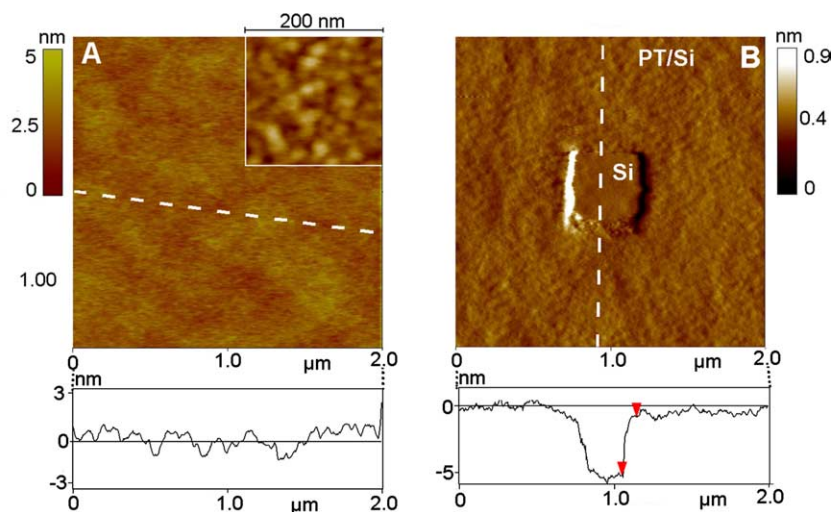


Fig. 3. AFM images of polytyramine films on silicon (ultrasonically cleaned  $p^{++}$ -Si (100)) prepared by electrochemical polymerisation using a scan rate of  $100 \text{ mV s}^{-1}$  and 10 deposition cycles. (A) Tapping mode height image (in air) of PT film on silicon, with cross-section graph. Inset shows typical morphological structures of film. (B) AFM deflection image (contact mode in air) from sample in (A) after scratching of PT film using higher loading force ( $>50 \text{ nN m}^{-1}$ ). The cross-section graph obtained from image was used for determination of the film thickness.

high ( $50 \text{ nN m}^{-1}$ ) loading force contact mode AFM, we were able to scratch a region of the PT film and subsequently image a larger area including the scratched region (Fig. 3B). From the cross-section graph, we were able to determine a film thickness of approximately 5 nm.

### 3.3. Influence of silicon surface pre-treatments on the electropolymerisation process

In general, the formation of polymer films initiated electrochemically can be influenced by many parameters including: electrode properties (such as its conductivity and roughness), monomer concentration, solvent, supporting electrolyte, temperature and applied electrochemical methods and conditions [31]. Here, we investigate only the influence of electrode pre-treatment and its resistivity. We used three cleaning procedures for highly doped (low resistivity) silicon, which includes sonication, sonication/Piranha treatment and sonication/ $\text{NH}_4\text{F}$  treatment. Whilst acid treatment results in a high density of silanol and silicon oxide groups,  $\text{NH}_4\text{F}$  exposure leads to a hydride-terminated surface [32].

Fig. 4A shows the first CV scan for Piranha and fluoride treated silicon, respectively. Our first concern was that acid/peroxide treated silicon may lead to the formation of a thick oxide layer which could block electron-transfer at the electrode interface and minimise oxidation of tyramine monomer in solution. However, CVs of tyramine polymerisation on Piranha treated were almost indistinguishable from the ones in Fig. 1. Electropolymerisation on silicon pre-treated with  $\text{NH}_4\text{F}$  solution (Si-H) revealed two differences in the CV. The first is a broader oxidation peak and slight shift of the oxidation potential to a more negative value (0.9–1.0 V) whilst the second is that a higher value of Faradaic charge was produced during the electropolymerisation in comparison with ultrasonically and acid/peroxide cleaned silicon. This is expected as the Si-H surface is more conductive than the surface covered with oxide layer, which allows for a more efficient charge transfer and therefore the oxidation of tyramine peaks at a lower potential. Alas, the Si-H terminated surface is easily oxidised under the conditions of electropolymerisation. Fig. 4B presents CVs (first scan) of a H-terminated silicon

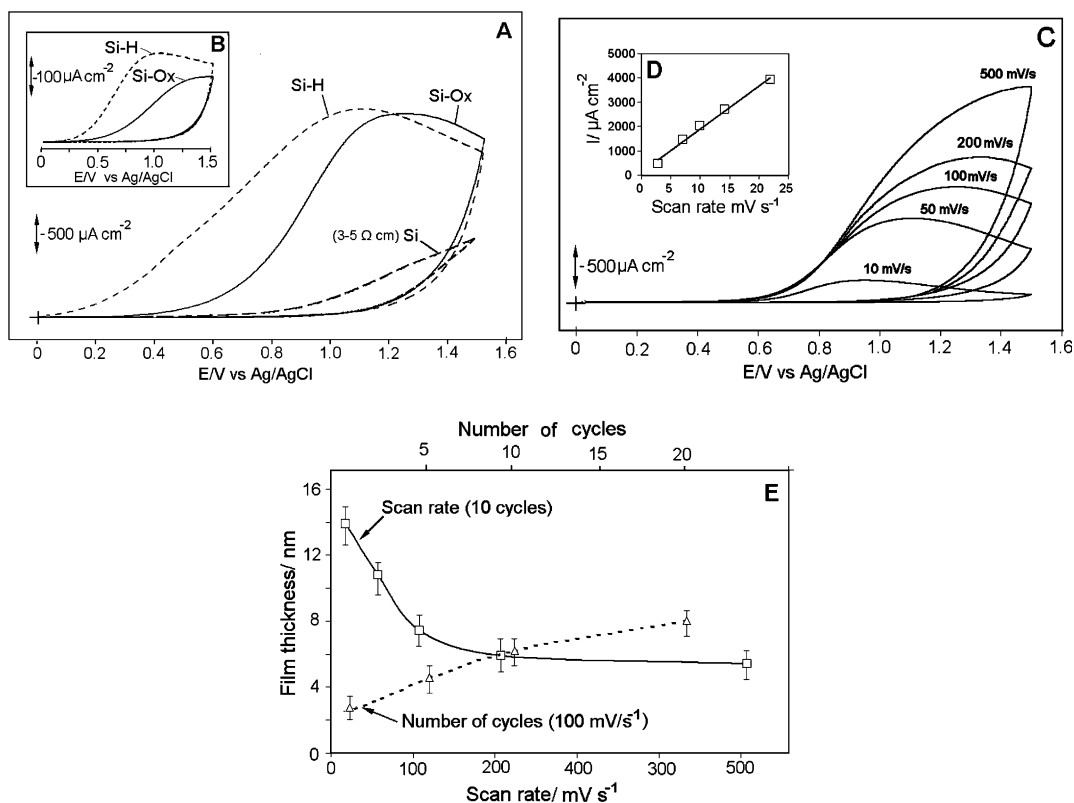


Fig. 4. (A) Cyclic voltammograms (first scan) for the electropolymerisation process of tyramine onto highly doped silicon ( $p^{++}$ -Si (100)) prepared by two treatments: oxidation in Piranha solution (—) and etching in  $\text{NH}_4\text{F}$  solution (---) and ultrasonically cleaned p-type ( $3\text{--}5\ \Omega\ \text{cm}$ ) silicon (---). Polymerisation conditions were the same as in Fig. 1. (B) Comparative cyclic voltammograms (first scan) for  $p^{++}$ -Si surfaces in supporting electrolyte (phosphate/methanol) without tyramine obtained at a scan rate of  $100\ \text{mV s}^{-1}$  versus Ag/AgCl. Influence of scan rate on polytyramine polymerisation process (ultrasonically cleaned silicon). (C) Cyclic voltammograms (first scan) obtained at scan rates of 10, 50, 100, 200 and  $500\ \text{mV s}^{-1}$  and (D) dependence of anodic oxidation current (taken from first scan) on the square root of scan rate. (E) Corresponding film thickness of PT film obtained using different scan rates and number of deposition cycles (thickness data obtained by ellipsometry).

surface and acid/peroxide oxidised silicon in buffer without tyramine. A broader and higher anodic current peak for H-terminated silicon compared to acid/peroxide oxidised silicon (or ultrasonically cleaned silicon, Fig. 1B) is evident. The oxidation process on a Si-H electrode started at a lower potential (0.25 V) and peaked at about 1.0 V. Silicon oxidation is also corroborated by an increase in oxygen content in XPS after performing a CV. These results show that both reduced resistivity and silicon electrooxidation contribute to the charge transfer on Si-H terminated electrodes and to the observed peak broadening. The fact that two parallel electrochemical pro-

cesses are occurring will have an impact on the polymer growth mechanism and this will require further investigation. Attempts to suppress Si oxidation during polymerisation by spiking the tyramine solution with hydrofluoric acid were unsuccessful.

To prove that high doping levels are essential for successful electropolymerisation, experiments were also performed using higher resistivity p-type silicon (p-Si,  $3\text{--}5\ \Omega\ \text{cm}$ ). The CVs in the presence of tyramine shows the absence of distinctive current peaks, a dominantly capacitive current and the absence of Faradic processes (Fig. 4A, bold dashed line). Hence, high resistivity silicon turned

out to be an inappropriate substrate electrode for electrodeposition of PT films.

### 3.4. Control over film thickness

A notable advantage of electrochemical methods for surface modification is the ability to control polymer growth on the surface and achieve a film with reproducible thickness and morphological properties. We performed electropolymerisations of tyramine by varying the scan rate from 10 to 500 mV s<sup>-1</sup> and the number of deposition cycles from 1–20. Fig. 4C shows a series of first cycle CVs of tyramine electropolymerisations on silicon (ultrasonically cleaned) at different scan rates. Electrochemical data (maximum oxidation potentials,  $E_{\max}$  and current densities) obtained from CVs and the corresponding data for film thickness and surface coverage obtained from ellipsometric measurements and AFM is provided in Table 1. We observed that increasing the scan rate led to an increase of oxidation potential (from +0.9 V to +1.4 V) and an increase in the anodic peak current (Fig. 4D). The graph shows a linear dependence of current with square root of scan rate, which is indicative of a diffusion controlled electrochemical process. From the Faradaic charge associated with the oxidation peak seen on CVs it is apparent that increased amounts of PT are deposited with decreasing scan rates. This was corroborated by thickness measurements by ellipsometry and AFM (Fig. 4E and Table 1). As expected, thickness increased with increasing number of cycles, although the anodic current and therefore the polymer deposition rate decreased with successive scans. The lower and upper limit of film thickness obtained by variation of scan rate and

Table 2

XPS elemental analysis of PT films on silicon (p<sup>++</sup> (100)) at different photoemission angles

Angle [°]	Surface atomic composition [%]			
	C	O	N	Si
0	73.6	14.7	6.0	5.7
70	82.7	11.0	5.1	1.2

number of deposition cycles was 2 nm and 15 nm, respectively.

### 3.5. Electrochemical stability and passivating properties of PT films

The development of PT/Si based platforms for biosensing or drug delivery required us to characterise the adherence, the chemical stability towards organic solvents and acids/bases as well as the electrochemical properties. We have found the PT film to be well adherent to the silicon substrate as judged by tape test experiments. Furthermore, films withstood incubation in strong acids, bases as well as organic solvents including ethanol, acetone and toluene. In the context of this work, the electrochemical stability of PT films was more thoroughly investigated. PT films (scan rate of 100 mV s<sup>-1</sup> and 20 cycles) on silicon were subjected to potential cycling in electrolyte using a large potential window (from -1.4 to +1.5 V). The CVs of the first 10 cycles (Fig. 5A) show exponential curve shape. Neither the desorption peak, reduction or oxidation peaks of the underlying silicon are observed, which indicates that the PT film on Si constitutes an electrochemically inactive and pinhole-free layer on the silicon electrode. Surprisingly, successive cycling did not lead to film degradation.

Table 1

Assessment of PT films electropolymerised on silicon (ultrasonically cleaned p<sup>++</sup>-Si (100)) at different scan rates

Scan rate [mV s <sup>-1</sup> ]	$E_{\max}$ [V]	Current density [ $\mu\text{A cm}^{-2}$ ]	Film thickness [nm]	Surface coverage [ $\text{mg m}^{-2}$ ]
10	0.95	470	14.4	15.84
50	1.11	1455	11.7	12.87
100	1.18	2020	7.9	8.69
200	1.24	2710	6.5	7.15
500	>1.4	>3920	6.2	6.82

Maximum oxidation potentials and current density were taken from the first scan. Thickness and surface coverage data were obtained by ellipsometry for PT film after 10 deposition cycles.

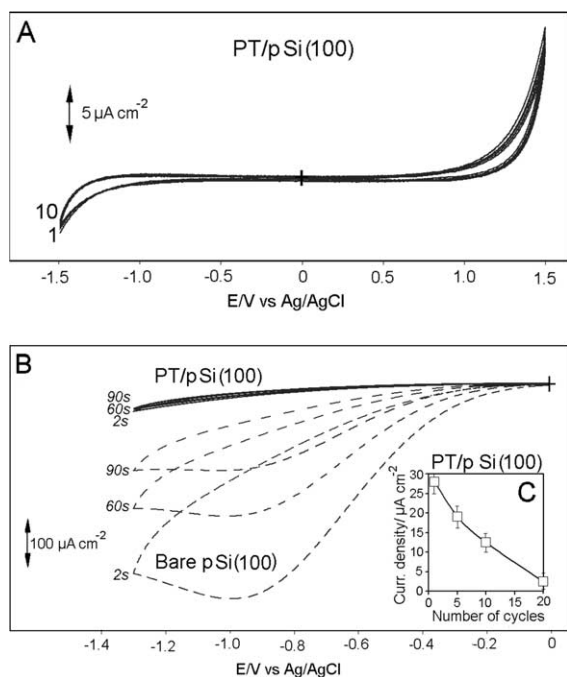


Fig. 5. Electrochemical stability studies of PT films on silicon ( $p^{++}$ -Si (100)) prepared using 20 deposition cycles and a scan rate of  $100 \text{ mV s}^{-1}$ . (A) Successive voltammograms (10 cycles is shown) using a potential window between  $-1.5 \text{ V}$  and  $1.5 \text{ V}$  versus Ag/AgCl in  $0.1 \text{ M}$  phosphate buffer ( $\text{pH } 7.0$ ). (B) Three successive cyclic voltammograms on bare silicon and PT/Si film in ferricyanide solution ( $0.1 \text{ mM}$  in  $0.2 \text{ M}$  KCl) and a scan rate of  $100 \text{ mV s}^{-1}$ . (C) Dependence of reduction current in ferricyanide solution on the number of PT deposition cycles.

To further investigate the integrity and surface passivating properties of PT films on silicon, we employed cyclic voltammetry measurements using ferricyanide as a redox probe [36]. Fig. 5B shows three successive CV cycles on bare Si (ultrasonically cleaned) and PT films on silicon, respectively, from  $0 \text{ V}$  to  $-1.3 \text{ V}$ . The CV for bare silicon shows a large diffusion-limited reduction peak with a maximum of  $-0.9 \text{ V}$ . Diffusion-limited electrochemistry at such large over-potentials is a typical feature on semi-conducting electrodes because the reduction of the solution species takes place via the hole injection into the silicon valence band [37]. The current dramatically decreases over three successive potential cycles, presumably because of the formation of an oxide layer on the silicon surface. In comparison, reduction current levels for PT on

Si are two orders of magnitude lower and remain stable. We attribute the remarkable stability and redox passivation of these films to the formation of a pinhole-free insulating layer. As expected, the reduction current of ferricyanide decreased with increasing number of deposition cycles and therefore with increasing film thickness (Fig. 5C).

### 3.6. Morphology of PT films on silicon

The influence of silicon surface treatment and electrochemical conditions (scan rate and cycle number) on the morphological characteristics of PT films was investigated by AFM. A typical AFM image (tapping mode in air) of a PT film prepared on silicon treated by  $\text{NH}_4\text{F}$  (Si-H terminated) (Fig. 6A) displays highly structured film topography with a mean roughness of  $4 \pm 1 \text{ nm}$ , which incidentally by far exceeds the roughness observed for PT films on ultrasonically and acid/peroxide cleaned silicon (Fig. 3A). Irregularly shaped nodules of  $70\text{--}100 \text{ nm}$  and an average height of  $5 \text{ nm}$  are apparent in higher resolution images (inset in Fig. 6A), larger in lateral and vertical dimensions than the globular structures observed for PT deposited on oxidised silicon. The different morphologies can be explained in terms of the observed differences in voltammetric behaviour, which are likely to influence polymer nucleation and growth. However, differences in surface energy, chemical composition of Si-H surface or roughness could also account for the differences in film morphology [38].

The influence of the number of deposition cycles on the resulting morphology of PT films on silicon was also further explored. A smooth (mean roughness  $0.53 \text{ nm} \pm 0.1 \text{ nm}$ ) topography with discrete or fused annular features and diameters of  $20\text{--}50 \text{ nm}$  and  $2\text{--}4 \text{ nm}$  in height was observed on a PT film prepared by one CV cycle (Fig. 6B). These 'donut'-shapes were more pronounced in phase images (inset Fig. 6B). The contrast in the phase channel between the donut ring and its centre are likely due to two different chemical environments, the dark regions (centre) corresponding to bare silicon or pinholes in this film. The presence of pinholes was expected as this film still shows

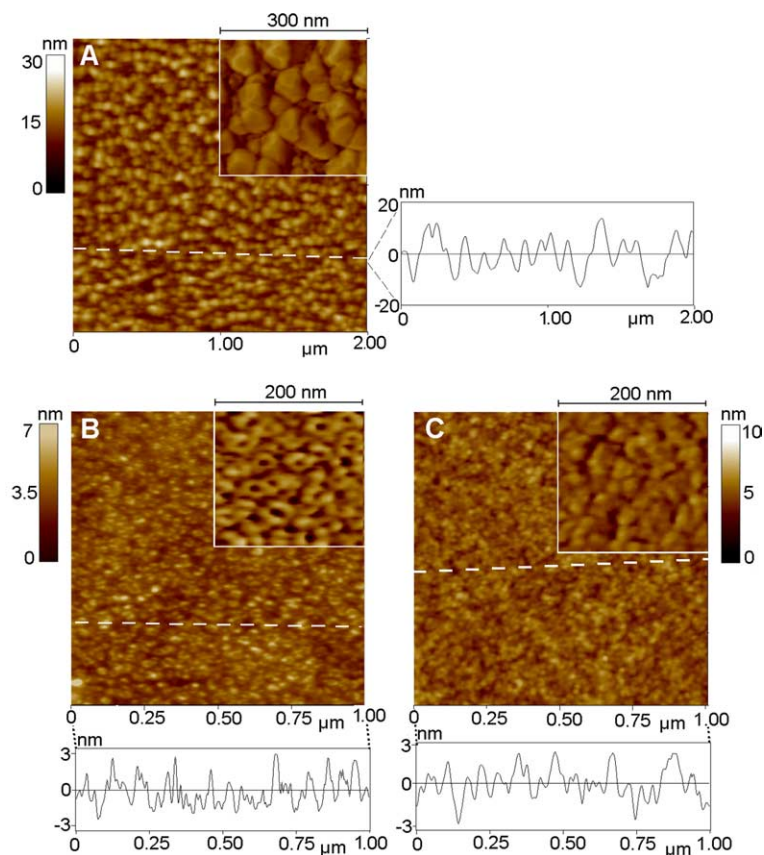


Fig. 6. AFM images (tapping mode in air) of PT films on silicon ( $p^{++}$ -Si (100)). The corresponding cross-sections are shown below the image. The inset corresponds to zoom-ins in the phase channel. (A) PT film prepared by electrochemical polymerisation on  $\text{NH}_4\text{F}$  treated silicon using a scan rate of  $100 \text{ mV s}^{-1}$  and 10 cycles. (B) PT film on silicon (ultrasonically cleaned) prepared at  $100 \text{ mV s}^{-1}$  and 1 cycle and (C) PT film on silicon (ultrasonically cleaned) prepared at  $100 \text{ mV s}^{-1}$  and 20 cycles.

high permeability towards the redox probe (Fig. 5C). These initial structures are likely to become nucleation sites for further polymer growth. Rather than rings, we had anticipated the formation of globular structures. However, the interplay of electrostatic effects between the positively charged tyramine and the—at pH 6.8—negatively charged silicon surface as well as stabilising intermolecular forces such as  $\pi$ - $\pi$  stacking, could lead to the condensation of tyramine oligomers on the electrode surface forming annular assemblies. By increasing the number of cycles (Fig. 3A), globular polymer deposits formed along with a decrease of the mean roughness from  $0.53 \text{ nm} \pm 0.1 \text{ nm}$  to  $0.35 \text{ nm} \pm 0.1 \text{ nm}$ . These observations point to-

wards a difference in the mechanism of polymer growth between the first and subsequent scans. An AFM image of a PT film electrochemically deposited on silicon using 20 cycles as shown in Fig. 6C. The enlarged phase image (inset) reveals its ultrastructure consisting of both spherical and rod-like nodules between 15 and 40 nm in lateral dimensions and a height of 2–3 nm, but given the size of these structures, we cannot rule out tip convolution artefacts [39]. After several cycles, charge transfer and formation of monomer radicals on the electrode surface is minimised by the insulating film and polymer growth is likely initiated by existing activated monomers and oligomers in solution.

### 3.7. Patterning of PT films on silicon

Whilst the ability to deposit thin organic films containing functional groups on silicon is useful, an even more important aspect of silicon device fabrication is the prospect of patterning. We have shown that PT film formation can be inhibited on medium resistivity p-type silicon. We also found that UV irradiation of the silicon surface passivated the electrode and prevented electropolymerisation. Based on those results, we have considered patterning electropolymerised PT films by generating oxide-passivated regions on a  $p^{++}$  silicon wafer. UV irradiation of a Si–H terminated  $p^{++}$  silicon wafer through a contact mask was used to produce regions with an insulating silicon oxide layer with thickness of more than several hundreds of nanometers [40]. This primed surface was then subjected to cyclic voltammetry in the presence of tyramine. Light microscopy assessment of this surface revealed a brightness contrast (Fig. 7), due to spatially controlled PT deposition. The lines (light) correspond to PT coated areas, whilst the dark squares correspond to uncovered silicon. This was confirmed by AFM (data not shown). These preliminary results demonstrate that UV induced silicon oxidation can be used to prepare patterned polymer films on silicon by electrochemical polymerisation. Work is underway to further characterise these patterned films and to use this strategy for

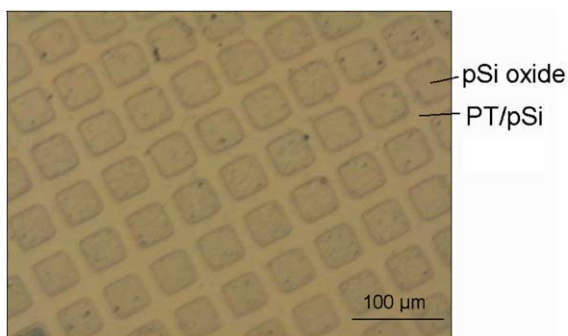


Fig. 7. Optical microscopy image of patterned PT film on silicon ( $p^{++}$ -Si (100)) prepared by UV lithography of Si–H terminated silicon ( $p^{++}$ -Si) and subsequent electropolymerisation of tyramine ( $100 \text{ mV s}^{-1}$  and 20 cycles). The light areas correspond to the PT film deposited while the dark areas correspond to the silicon oxide surface.

fabrication of integrated PT structures using SAMs and other polymers and explore their practical applications as platforms for drug delivery and sensing devices.

## 4. Conclusions

We have demonstrated for the first time that ultrathin polytyramine films can be formed electrochemically on low resistivity p-type silicon wafers using cyclic voltammetry. The electropolymerisation of tyramine was successfully carried out on both Si–H terminated and oxidised silicon surfaces. The low resistivity of p-silicon was found to be essential for the deposition of PT films. The electrooxidation of silicon and formation of silicon oxide was observed during the electropolymerisation process, but did not inhibit the tyramine oxidation process and polymer growth on the surface. Changing the scan rate and number of cycles demonstrated the ability to reliably control the thickness of PT films from a few nm to more than 15 nm. The formation of ultrathin PT films on silicon was verified by XPS, AFM, ellipsometry and electrochemical methods. The film showed good electrochemical stability in buffer solution (pH 6.8) over a wide potential range ( $-1.5 \text{ V}$  to  $+1.5 \text{ V}$ ) and good passivating properties. Using XPS, we confirmed the presence of amino groups within the PT film and the absence of oxidised nitrogen species. The introduction of defined interfacial functionalities provides an important starting point for further studies of covalent attachment of biomolecules with a view towards biosensing applications. Furthermore, we demonstrate a simple patterning method for PT films on silicon. Finally, it should be feasible to incorporate drugs or biomolecules into the film during polymerisation under the mild experimental conditions described here without affecting drug/biomolecule activity. This has potential applications in controlled drug delivery.

## Acknowledgments

The authors acknowledge support from Flinders University and the Australian Research

Council. We thank Dr. J.J. Gooding from UNSW for his useful suggestions on the manuscript.

## References

- [1] J.T. Yates, *Science* 279 (1998) 335.
- [2] A. Ulman, *Introduction to Thin Organic Films: From Langmuir Blodgett to Self-assembly*, Academic Press, Boston, MA, 1991.
- [3] A.B. Sieval, A.L. Demirel, J.W.M. Nissink, M.R. Linford, J.H. van der Maas, W.H. de Jeu, H. Zuilhof, E.J.R. Sudholter, *Langmuir* 14 (1998) 1759.
- [4] J.M. Buriak, *Chem. Commun.* (1999) 1051.
- [5] Z.H. Yang, P. Zhang, D.J. Whang, D. Zhang, X.D. Chai, T.J. Li, *Synth. Metals* 85 (1997) 1293.
- [6] I. Musa, W. Eccleston, *Thin Solid Films* 344 (1999) 466.
- [7] M. Herlem, B. Fahys, G. Herlem, B. Lakard, K. Reybier, A. Trokourey, T. Diaco, S. Zairi, N. Jaffrezic-Renault, *Electrochim. Acta* 47 (2002) 2597.
- [8] K. Norrman, K.B. Haugshoj, N.B. Larsen, *J. Phys. Chem. B* 106 (2002) 13114.
- [9] X. Kong, T. Kawai, J. Abe, T. Iyoda, *Macromolecules* 34 (2001) 1837.
- [10] K. Kim, M.Y. Jung, G.L. Zhong, J.-I. Jin, T.Y. Kim, D.J. Ahn, *Synth. Metals* 144 (2004) 7.
- [11] S.A. Emr, A.M. Yacynych, *Electroanalysis* 7 (1995) 913.
- [12] R.J. Geise, J.M. Adams, N.J. Barone, A.M. Yacynych, *Biosensors Bioelectron.* 6 (1991) 151.
- [13] E.C. Venancio, C.A.R. Costa, S.A.S. Machado, A.J. Motheo, *Electrochem. Commun.* 3 (2001) 229.
- [14] M. Situmorang, J.J. Gooding, D.B. Hibbert, D. Barnet, *Biosensors Bioelectron.* 13 (1998) 953.
- [15] V.A. Myamlin, Y.V. Pleskov, *Electrochemistry of Semiconductors*, Plenum Press, New York, 1967.
- [16] A.G. Muñoz, M.M. Lorengel, *J. Solid, State Electrochem.* 6 (2002) 513.
- [17] C. Gurtner, A.W. Wun, M.J. Sailor, *Angew. Chem. Int. Ed.* 38 (1996) 1999.
- [18] E.G. Robins, M.P. Stewart, J.M. Buriak, *Chem. Commun.* (1999) 2479.
- [19] A. Teyssot, A. Fidélis, S. Fellah, F. Ozanam, J.-N. Chazalviel, *Electrochim. Acta* 47 (2002) 2565.
- [20] H. Grisar, Y. Cohen, D. Aurbach, C.N. Sukenik, *Langmuir* 17 (2001) 1608.
- [21] C. Steinem, A. Janshoff, V.S.-Y. Lin, N.H. Völcker, M.R. Ghadiri, *Tetrahedron* 60 (2004) 11259.
- [22] E. Szili, H. Thissen, J.P. Hayes, N.H. Voelcker, *Biosensors Bioelectron.* 19 (2004) 1395.
- [23] E. Szili, H. Thissen, J.P. Hayes, J. Shapter, N.H. Voelcker, *Proc. SPIE* 4937 (2002) 211.
- [24] M.C. Pham, P.C. Lacaze, J.E. Dubois, *J. Electrochem. Soc.* 131 (1984) 777.
- [25] L.D. Tran, B. Piro, M.C. Pham, T. Ledoan, C. Angiari, L.H. Dao, F. Teston, *Synth. Metals* 139 (2003) 251.
- [26] M. Situmorang, J.J. Gooding, D.B. Hibbert, *Anal. Chim. Acta* 394 (1999) 211.
- [27] M. Situmorang, J.J. Gooding, D.B. Hibbert, D. Barnet, *Electroanalysis* 13 (2001) 1469.
- [28] D. Losic, J.G. Shapter, J.J. Gooding, *Electrochem. Comm.* 4 (2002) 953.
- [29] D. Losic, J.G. Shapter, J.J. Gooding, *J. Solid State Electrochem.*, in press, doi:10.1007/S10008-004-0614-X.
- [30] S. Tanuma, C.J. Powell, D.R. Penn, *Surf. Interf. Anal.* 21 (1993) 165.
- [31] X.-G. Li, M.-R. Huang, W. Duan, *Chem. Rev.* 102 (2002) 2925.
- [32] G.J. Pietsch, U. Köhler, M. Henzler, *J. Appl. Phys.* 73 (1993) 4797.
- [33] D. Losic, J.J. Gooding, J.G. Shapter, D.B. Hibbert, K. Short, *Electroanalysis* 13 (2001) 1385.
- [34] H. Mori, A. Böker, G. Krausch, A.H.E. Müller, *Macromolecules* 34 (2001) 6871.
- [35] D. Losic, J.J. Gooding, J.G. Shapter, *Langmuir* 17 (2001) 3307.
- [36] C.J. Barlet, D.B. Robinson, J. Cheng, T.P. Hunt, C.F. Quate, C.E.D. Chidsey, *Langmuir* 17 (2001) 3460.
- [37] P.M.M.C. Bressers, S.A.S.P. Pagano, J.J. Kelly, *J. Electroanal. Chem.* 391 (1995) 159.
- [38] G.S. Higashi, Y.J. Chabal, G.W. Trucks, K. Ragavachari, *Appl. Phys. Lett.* 56 (1990) 656.
- [39] S.S. Sheiko, M. Moller, A.M.C. Reuvekamp, H.W. Zandbergen, *Phys. Rev. B* 48 (1993) 5675.
- [40] T.E. Orlowski, D.A. Manteli, *J. Appl. Phys.* 64 (1988) 4410.